Chemical Engineering Science 255 (2022) 117657

Contents lists available at ScienceDirect

Chemical Engineering Science

journal homepage: www.elsevier.com/locate/ces

Continuous flow nitration of 3-[2-chloro-4-(trifluoromethyl) phenoxy] benzoic acid and its chemical kinetics within droplet-based microreactors

Shenfang Li [a], Xunli Zhang [b], Desheng Ji [a], Qingqiang Wang [a], Nan Jin [a], Yuchao Zhao [a,*]

[a] Shandong Engineering Research Center of Green Manufacturing for New Chemical Materials, College of Chemistry & Chemical Engineering, Yantai University, Yantai 264005, China
[b] School of Engineering & Institute for Life Sciences, University of Southampton, Southampton SO17 1BJ, UK

HIGHLIGHTS

- The synthesis of Acifluorfen by continuous flow nitration was performed within droplet-based microreactor.
- The effects of operating parameters were characterized by hydrodynamics and thermodynamics.
- The apparent and intrinsic kinetic model was established.

GRAPHICAL ABSTRACT

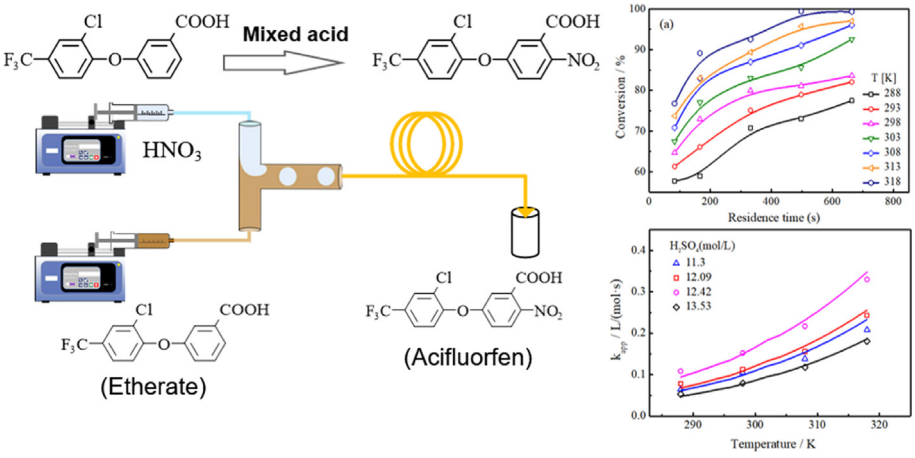

ARTICLE INFO

Article history:
Received 15 January 2022
Received in revised form 28 March 2022
Accepted 4 April 2022
Available online 9 April 2022

Keywords:
Microreactors
Microchannel
Continuous flow
Nitration
Kinetics
Mass transfer

ABSTRACT

Aromatic nitration still faces unmet technical challenges in relation to being heterogeneous and highly exothermic. In this work, a continuous flow aromatic nitration was developed with mixed acid within droplet-based microreactors. The effects of key operating parameters were characterized on the nitration of 3-[2-chloro-4-(trifluoromethyl)phenoxy] benzoic acid. The optimized reaction temperature, M-ratio and N/S were found to be 308 K, 1.6 and 0.57, respectively. Under these conditions, a conversion of 83.03% and selectivity of 79.52% were achieved. The addition of acetic anhydride improved both the solubility of etherate in the organic phase and the absorbability of water produced from the reaction, leading to increase in conversion, however increased by-products accordingly with reduced selectivity. Pseudo-homogeneous kinetics models were developed of apparent and intrinsic reaction rate constant, supporting the second-order reaction assumption. The calculated results based on the kinetics model were found to be in good agreement with the experimental results.

* Corresponding author.
E-mail address: yczhao@ytu.edu.cn (Y. Zhao).

https://doi.org/10.1016/j.ces.2022.117657
0009-2509/

Nomenclature

A	pre-exponential factor, $m^3/(mol{\cdot}s)$
a	activity, $mol{\cdot}L^{-1}$
C_A	concentration of etherate, $mol{\cdot}L^{-1}$
C_A^0	initial concentration of etherate, $mol{\cdot}L^{-1}$
$C_{NO_2^+}$	concentration of the nitronium ion, $mol{\cdot}L^{-1}$
C_{HNO_3}	concentration of nitric acid, $mol{\cdot}L^{-1}$
$C^t_{HNO_3}$	total concentration of nitric acid, $mol{\cdot}L^{-1}$
C_{H^+}	proton concentration in the mixed acid, $mol{\cdot}L^{-1}$
$C_{H_2SO_4}$	concentration of the sulfuric acid, $mol{\cdot}L^{-1}$
D	diameter of microchannel, m
$D_{Etherate}$	diffusivity of Etherate, $m^2{\cdot}s^{-1}$
d	diameter of droplets in microchannel reactor, m
Etherate	3-[2-chloro-4-(trifluoromethyl)phenoxy] benzoic acid
Ea	activation energy, $kJ{\cdot}mol^{-1}$
ΔG_{HNO_3}	gibbs free energy of HNO_3, $kJ{\cdot}mol^{-1}$
Ha	Hatta number
k_{app}	apparent reaction rate constant, $L{\cdot}mol^{-1}{\cdot}s^{-1}$
k^*_{exp}	apparent rate constant of the nitronium ion, $L{\cdot}mol^{-1}{\cdot}s^{-1}$
k_L	overall mean mass transfer coefficient, $m{\cdot}s^{-1}$
k_0	intrinsic reaction rate constant, $L{\cdot}mol^{-1}{\cdot}s^{-1}$
K_{HNO_3}	equilibrium constant of nitric acid
$K_{NO_2^+}$	equilibrium constant of nitronium ion
M-ratio	molar ratio of nitric acid to etherate
M_c	activity coefficient function
N/S	molar ratio of nitric acid to sulfuric acid
n_A	the amount of substance of etherate, mol
n	the thermodynamic parameter defined in Eq.11
Pe	Peclet number of the mixed acid phase
Q	total flow rate, $\mu L{\cdot}min^{-1}$
Q_c	flow rate of the continuous phase, $\mu L{\cdot}min^{-1}$
Q_d	flow rate of the dispersed phase, $\mu L{\cdot}min^{-1}$
Re	Reynolds number of the mixed acid phase
Sc	Schmidt number of mixed acid phase
Sh	Sherwood number of mixed acid phase
T	reaction temperature, K
t	reaction time, s
v_m	molecular volume of Etherate at normal boiling point, m^3/mol
$v_{Organic}$	flow rates of organic phase, $\mu L{\cdot}min^{-1}$
$v_{Mixed\ acid}$	flow rates of mixed acid, $\mu L{\cdot}min^{-1}$
w	mass fraction of etherate in organic phase
x_A	conversion of etherate

Greek letters

$\rho_{Organic}$	density of etherate, $g{\cdot}ml^{-1}$
ρ	density of sulfuric acid, $g{\cdot}ml^{-1}$
γ_A	activity coefficients of etherate
$\gamma_{NO_2^+}$	activity coefficients of NO_2^+
γ^*	activity coefficient of the transition-state intermediate
μ	viscosity, Pa·s

1. Introduction

Aromatic nitration is a class of reactions that are widely applied in the synthesis of industrially important chemical intermediates involved in the production of dyes, plastics, herbicides and pharmaceuticals (Vogt et al., 2015). However, technical challenges still remain in further improvement of the industrial process. Firstly, as the nitration reagent is typically a mixture of concentrated nitric and concentrated sulfuric acid, it constitutes a heterogeneous liquid–liquid two-phase reaction system (Rahaman et al., 2010). In this heterogeneous system, the reaction can take place either mostly in the aqueous phase or at the two-phase interface where effective mass transfer across interface is essential (Schöfield, 1980; Olah et al., 1989). Secondly, aromatic nitration reactions are mostly highly exothermic with fast reaction rates, where the reaction enthalpy ranges typically from -73 $kJ{\cdot}mol^{-1}$ to -253 $kJ{\cdot}mol^{-1}$, largely depending on the functional groups on the aromatic ring and their positioning (Sharma et al., 2015; Wen et al., 2017). In addition, the combination of these factors and their interplay add further complexity and challenges to the reaction system for achieving high safety and efficiency. For example, in the most commonly used batch reactors currently, poor mass transfer can result in locally excess nitric acid that, in turn, leads to the formation of localized "hot spots" and side reactions such as secondary and tertiary nitration for by-products (Sharma et al., 2015). Therefore, there has been much effort in addressing these challenges by developing safer and more efficient reactors for aromatic nitration.

Over the last two decades, the development in microreactor technology has demonstrated its unique advantages, compared to conventional macroscale batch reactor systems, owing to its large specific surface area, excellent mass and heat transfer rate (Wang et al., 2011), intrinsic process safety, accurate control over reaction parameters, high integration and scalability (Hessel et al., 2011). The submillimeter microscale continuous flow process is particularly of significance to fast exothermic and complex reactions, such as polymerization and radical reactions involving unstable intermediates or toxic reagents (Kim et al., 2004; Zaborenko et al., 2010). In our series of studies on microreactor technology, we have successfully developed a range of droplet-based microreactors, demonstrating the capability and suitability for effective multiphase reactions by regulating hydrodynamics, interface characteristics and overall mass transfer (Zhang et al., 2018; Ma et al., 2019; Zhou et al., 2020; Hao et al., 2020; Sun et al., 2021; Jin et al., 2021). Furthermore, microreactors have been shown as a promising platform for the characterization of chemical reaction kinetics, mainly due to the high degree of controllability over the multiphase microenvironment (Zaborenko et al., 2010; McMullen and Jensen, 2011; Wang et al., 2011; Su et al., 2015).

With the unique characteristics of microreactors, the performance of high space time yield, short reaction time, low energy consumption, and high selectivity have also been demonstrated for carrying out aromatic nitration (Olah et al., 1989; Jähnisch et al., 2004; Coyle and Oelgemöller, 2008; Illg et al., 2010; Sharma et al., 2015). By using a continuous-mode microreactor, Kulkarni et al. (Kulkarni et al., 2009) realized the nitration of benzaldehyde with controllable reaction time, temperature and stoichiometric ratios. Yu et al. (Yu et al., 2013) developed a continuous microreactor process for the nitration of *p*-difluorobenzene with fuming nitric acid achieving a high product yield 98% within 2 min reaction time. Lan et al. (Lan and Lu, 2021) further developed a micropacked-bed reactor for the continuous nitration of *o*-dichlorobenzene which was impressively completed within 5 s with a selectivity of 89% for the main product. Considering the highly exothermic nature with high risk of explosion, the nitration reaction is normally performed at low temperature, typically around 273 K, which can inevitably increase operating difficulties and energy consumption. To address these issues, Wen et al.

(Wen et al., 2018) developed a microreactor for the nitration of trifluoromethoxybenzene by mixed acid, where the reaction temperature was increased to 271 K (being 8 K higher than that in the conventional batch process). For the nitration of 2-ethylhexanol with the mixed acid in a microreactor, Li et al. (Li et al., 2017) further raised the reaction temperature to room temperature which was significant compared to the commonly applied temperature range of 263 K to 283 K in batch reactors. In addition, the homogeneous nitration kinetics of aromatic compounds were well investigated by Luo's group (Cui et al., 2021, Song et al., 2022a, 2022b) using a continuous flow microreactor, where each experimental data could be obtained in a few seconds due to the accurate temperature control.

Among many important aromatic nitration products, fluorinated diphenyl ethers have been discovered to be effective herbicides with high biological activities and photostability, low toxicity to mammals, and low residue (Jiang, 2006), which are widely used agriculturally to control annual broadleaf weeds in crop fields. Acifluorfen, in particular, has been found suitable in fields growing soybeans, peanuts, peas, and rice as these crops naturally have a high tolerance to acifluorfen and its salts (Shepherd et al., 2013). Currently, acifluorfen is mostly produced with conventional batch reactors through the nitration of 3-[2-chloro-4-(trifluoromethyl)phenoxy] benzoic acid with mixed nitric and sulfuric acids (Giacobbe and Tsien, 1983), as expressed in Eqs. (1)–(4).

$$HNO_3 + 2H_2SO_4 \rightarrow NO_2^+ + 2HSO_4^- + H_3O^+ \quad (1)$$

$$C_{14}H_8ClF_3O_3 + NO_2^+ \rightarrow C_{14}H_8ClF_3NO_5 + H^+ \quad (2)$$

$$2HSO_4^- + H_3O^+ + H^+ \rightarrow 2H_2SO_4 + H_2O \quad (3)$$

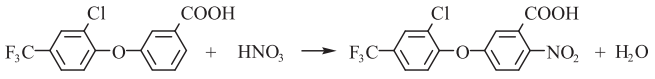

(4)

In the conventional batch process, the reaction temperature range of 273–278 K is generally selected while the mixed acid has to be added dropwise into the reactor over a lengthy period of feeding time, typically 2–4 h, that is followed by a further >5 h reaction time to complete the reaction (Jiang, 2006). Clearly, these constrains have impact significantly on the space time yield of the reactor and the efficiency of the overall process. Despite the importance of this product commercially and agriculturally, the fundamental drawbacks of macroscale batch reactors together with the remarkable lack of kinetics data for this particular reaction still hinder the progress for improving the process towards economically viable and environmentally sustainable manufacturing.

The aim of the present research was to develop a continuous flow process for aromatic nitration with mixed acid towards the production of acifluorfen, while gain insights into the chemical kinetics of the reaction, by using droplet-based microreactor technology that has been intensively developed in our previous work. Through selected design of the droplet-based microreactor, the nitration of 3-[2-chloro-4-(trifluoromethyl)phenoxy] benzoic acid with mixed (HNO_3/H_2SO_4) acid was carried out in the continuous flow droplet format. The reaction conditions were optimized by quantifying the effects of a wide range of key operating parameters, including reaction temperature, residence time and total flow rate, molar ratio of HNO_3 to H_2SO_4 (namely, N/S), molar ratio of HNO_3 to 3-[2-chloro-4-(trifluoromethyl) phenoxy] benzoic acid (namely, M-ratio), and the introduction of acetic anhydride into organic phase (mainly 1,2-dichloroethane) as a solubility promoter and also water absorbent. Three microreactor dimensions were also designed in order to assess the microreactor scalability. Furthermore, through theoretical analysis a pseudo-homogeneous based on the kinetics model was developed to determine kinetics parameters of the nitration reaction, which was further used to predict the reactant conversion. Finally, the kinetics model was validated by comparing calculated data against experimental results.

2. Experimental

2.1. Chemicals

Chemicals used in this work mainly included: fuming nitric acid (>98 wt%, Tianjin Kemiou Co., Ltd.), sulfuric acid (concentration > 95 wt%, Sinopharm Chemical Reagent Co., Ltd.), 3-[2-chloro-4-(trifluoromethyl) phenoxy] benzoic acid (>93.3 wt%, Qingdao Hansen Biologic Science Co., Ltd.), 1,2-dichloroethane (>99 wt%, Sinopharm Chemical Reagent Co., Ltd.), acetic anhydride (>99 wt%, Sinopharm Chemical Reagent Co., Ltd.), methanol (HPLC, Merck), acetic acid (HPLC, Sinopharm Chemical Reagent Co., Ltd.), phosphoric acid (HPLC, Sinopharm Chemical Reagent Co., Ltd.). The deionized water was made in-house. All chemicals and reagents were used as received without any further purification.

2.2. Experimental setup and procedure

The microreactor consisted mainly of a FEP T-mixer (i.d. 0.5 mm, IDEX Health & Science), two inlet PTFE tubes with sufficient length for preheating (i.d. 0.5 mm, length 1 m, IDEX Health & Science), and a main reaction circular PTFE channel with selected inner diameter and length (i.d. 0.5, 1.0, or 1.59 mm; length 0.4–8 m; Nichias Corporation). The microreactor and overall experimental setup is schematically shown in Fig. 1.

Two precision syringe pumps (Harvard 11 ELITE Single, USA) were used to deliver organic phase and the mixed acid through the respective inlet tube into the T-mixer, and then the main reaction channel. All inlet tubes, T-mixer and the reaction channel were placed in a thermostatic water bath (Julabo GmnH CORIO CD-200F, Germany) at preset reaction temperature. The residence time was regulated by the length of the reaction channel and/or flow rate. The M-ratio was controlled by the volumetric flow rate ratio of two phases. The reaction mixture from the outlet of the main reaction channel was then quenched in an ice-water bath (Julabo GmnH CORIO CD-200F, Germany). The organic phase was separated quickly from the quenched reaction mixture, and was subsequently treated with solvent removal by natural volatilization at room temperature, drying by a baking oven at 333 K, powder grinding to form final fine powder product. A stereo microscope (Olympuss ZX2-ILLK, Japan) coupled with a high-speed camera (Phantom Miro R311, USA) were used to record the droplet length and flow. The imaging frame rates was set as 1000 frames per second. The length and the distance of the acid droplets were measured by ImageJ.

2.3. Product analysis

For product analysis, the powder product was first dissolved in methanol that was then analyzed with HPLC (Waters e2695, 2998 PDA, Aglilent Eclipse Plus C18-5 μm 4.6 × 250 mm, UV-254 nm). The mobile phase was made of methanol (70 vol%) + water (30 vol%) + acetic acid (0.3 vol%) + phosphoric acid (0.2 vol%). The column temperature was kept at 308 K and the flow rate was set at 1 $mL{\cdot}min^{-1}$. The composition of product was quantitatively analyzed by the external standard method, and the molar concentration of total etherate was determined by the corrected

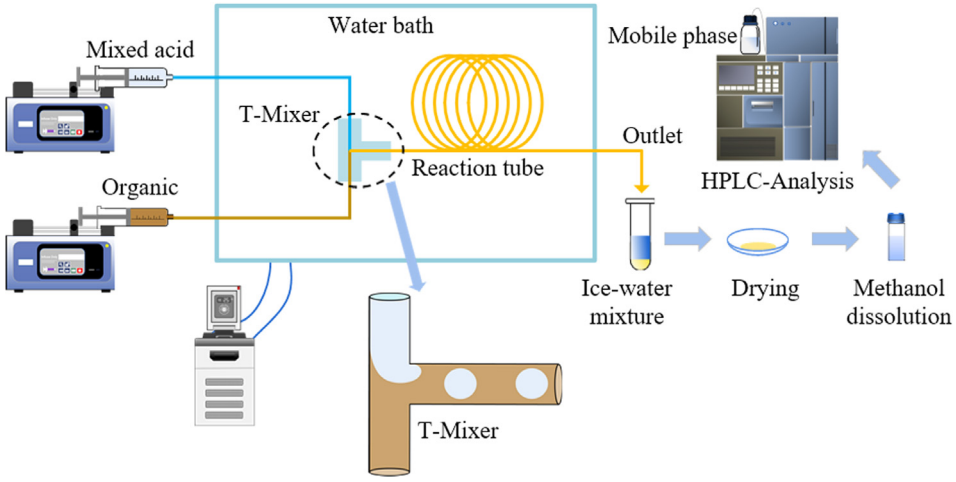

Fig. 1. Schematic overview of the experimental setup and operation flow.

peak area normalizing method. The conversion of etherate was calculated by the following equation:

$$x_A = \left(1 - \frac{c_{etherate}}{c_{total\ etherate}}\right) \times 100\% \quad (5)$$

where x_A is the conversion of etherate and c is the molar concentration of the substances in the sample.

The selectivity to acifluorfen was calculated by the following equations:

$$S = \left(\frac{c_{acifluorfen}}{c_{total\ etherate} - c_{etherate}}\right) \times 100\% \quad (6)$$

where S is the selectivity to the target product acifluorfen.

3. Results and discussion

3.1. Controllable droplet microfluidics coupled with nitration reaction

By varying total flow rate and flow rate ratio, stable and controllable droplet-based multiphase microfluidics was achieved, as shown in Fig. 2. Regular droplets were generated of aqueous phase mixed acid which were suspended in the continuous organic phase composed of mainly 1,2-dichloroethane as main carrier, and reactant 3-[2-chloro-4-(trifluoromethyl) phenoxy] benzoic acid (or etherate) whose mass fraction in the total mass of two fluid streams was 8.8 wt%. Because the solubility of the reactant in 1,2-dichloroethane is very low, especially as no acetic anhydride exists in the organic phase. In order to stably deliver the feed without solid particles, a large amount of solvent must be adopted in microreactor. Although the low content of reactant will reduce the production capacity, it is more important to carry out successfully the nitration process, control precisely the operating parameters and improve the stability of the product quality. Varying amount of acetic anhydride was also added to the organic phase to assist the dispersion of etherate in the organic phase and also act as a water absorbent in the mixed acid during the nitration reaction. In the mixed acid the water content was about 4.04–4.39 wt%, and the molar ratio of sulfuric acid to nitric acid (S/N) was varied between 0.41 and 0.75. The M-ratio was in the range of 0.9–2.0.

Under typical operating conditions, the size of aqueous droplets was in the range of 0.36–0.50 mm long, with a distance of 2.47–7.51 mm between adjacent droplets at the beginning of droplet formation (as illustrated in Fig. 2). The frequency of droplet generation was typically ranging from 2.07 Hz to 27.03 Hz.

Through initial experiments by changing a range of factors, some key operating parameters were identified, including reaction temperature, the residence time, total flow rate, M-ratio, N/S in the mixed acid, and acetic anhydride content in organic phase. The diameter of the reaction channel was found also an important factor affecting reaction results which was also of direct relevance to the production capacity. All these key parameters were subsequently investigated in more detail.

3.2. Optimization of key operating parameters

3.2.1. Effects of reaction temperature and residence time

For the heterogeneous nitration reaction, the reaction temperature and the residence time are important factors that affect the conversion of the reagents and the selectivity of the main product. Their effects were quantified by varying temperature (288–318 K) and residence time (60–660 s) in the reactor while keeping N/S at 0.57 in the mixed acid and an M-ratio of 1.6. The experimental results are depicted in Fig. 3.

As shown in Fig. 3(a), the conversion of etherate increased by increasing either residence time or reaction temperature. The former can be attributed to the longer contact time of the two reactant phases and longer reaction time. The latter was mainly due to the higher temperature resulting in higher reaction rate

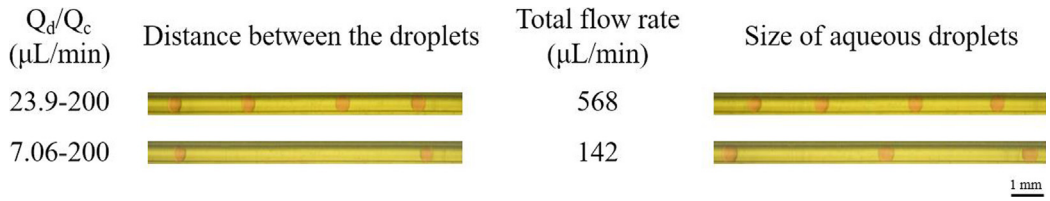

Fig. 2. Micrographs of droplet flow showing distance and size of aqueous droplets under different operating conditions.

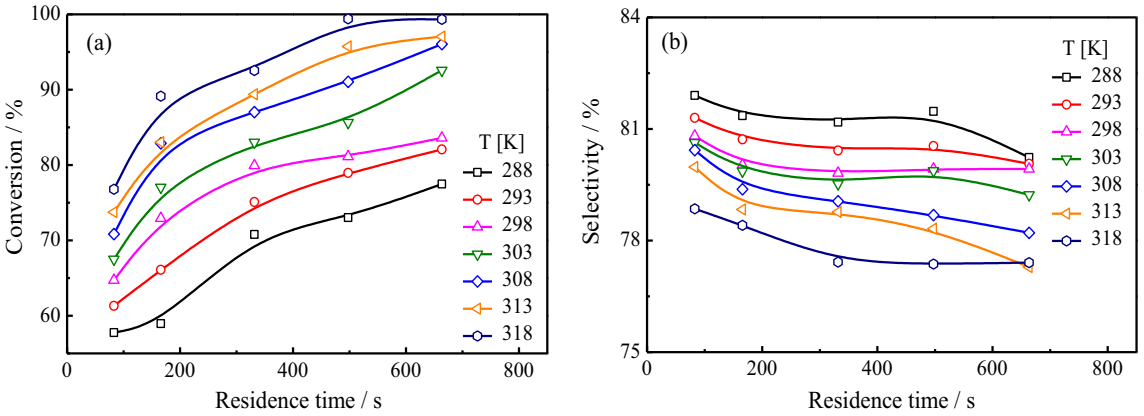

Fig. 3. Effects of reaction temperature and residence time on (a) conversion of etherate and, (b) product selectivity in nitrification. Etherate content in organic phase = 8.8 wt %, M-ratio = 1.6, N/S = 0.57, total flow rate = 142 μL·min^{-1}.

constants, whilst higher mass transfer rates across the two phases. Fig. 3(b) shows that the selectivity decreased with the increase of either reaction temperature or residence time, indicating the possible side reactions which were accelerated at higher temperatures and prolonged over longer reaction times.

As generally understood, the reaction rate coefficient increases with the increase of reaction temperature according to the Arrhenius equation. At the same time, the increase in temperature can enhance mass transfer across the multiphase interface, as the molecular diffusion coefficient is proportional to the reaction temperature, which can further increase the apparent reaction rate. When the residence time of the reagents in the microreactor was short (<300 s), the reaction was unable to complete, thus showed overall low conversions especially in the low temperature range. On the other hand, when a longer residence time was selected, it gave higher possibility of side reactions reducing the selectivity of the main product, as also observed in other reactions (Zeibi Shirejini and Mohammadi, 2017). For a balanced outcome, temperatures and residence times in the middle ranges (i.e. 298 K and 220 s) were selected in the subsequent investigations into the effects of other factors.

3.2.2. Effects of M-ratio and N/S in the mixed acid

By varying M-ratio (0.9–2.0) and N/S (0.41–0.75) in the mixed acid, their effects on reaction conversion and selectivity were investigated with a fixed temperature of 298 K and a residence time of 220 s. The results are illustrated Fig. 4.

As can be seen from Fig. 4(a), the conversion of etherate increased with the increase of M-ratio. That was largely due to the supply of more NO_2^+ ions at higher M-ratios. At the same time, the increase amount of sulfuric acid at higher M-ratios reduced the dilution effect of the reaction produced water during the reaction process. It was also observed that raising M-ratio in the feed increased the size of the dispersed acid droplets in the oil phase along the microchannels, causing the two-phase interfacial area to be reduced. The reduction in interfacial area can negatively affect the overall mass transfer performance and, in turn, the apparent reaction rate. However, the results in Fig. 4(a) suggested that under the experimental conditions this transport effect was insignificant on overall conversion where little signs of levelling-off were observed with conversion in the high M-ratio ranges.

At a given M-ratio level, overall, lower N/S ratios resulted in higher conversions. This may be attributed to the increased amount of sulfuric acid which acted as a catalyst in the nitration reaction to protonate nitric acid and generate NO_2^+ ions (Sharma et al., 2015). In addition, the increased amount of sulfuric acid as a water absorbent enhanced the inhibition of dilution effect of water produced from the nitration reaction, that further increased the apparent reaction rate (Ross et al., 1983; Deno et al., 1961). It was observed that, in the lower M-ratio range (<1) the effect of varying M-ratio was insignificant on conversion, as shown in Fig. 4(a). That was likely due to the slow production rate of NO_2^+ in the mixed acid with low sulfuric acid contents.

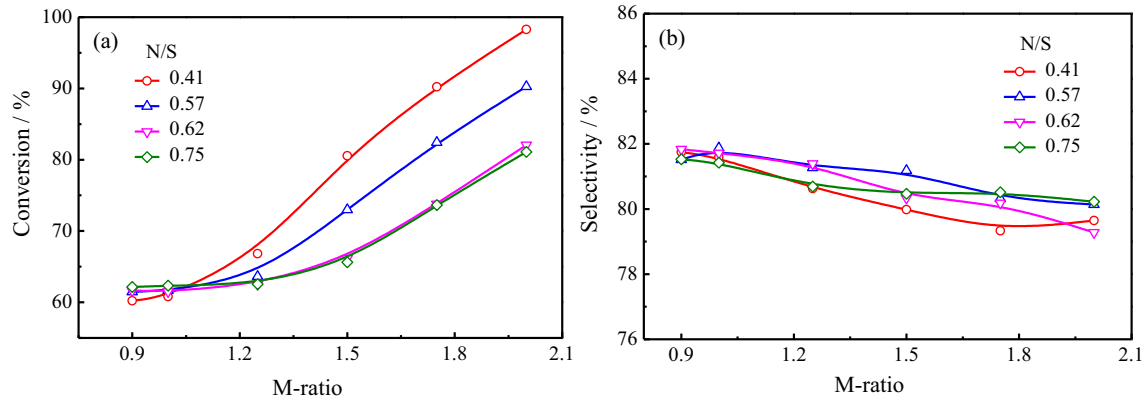

Fig. 4. Effects of M-ratio and N/S in mixed acid on (a) conversion of etherate and, (b) product selectivity in nitrification. Etherate content in organic phase = 8.8 wt%, temperature = 298 K, residence time = 220 s, reaction tube length = 4 m.

Fig. 4(b) shows that overall the product selectivity decreased slightly with increasing M-ratio, dropping from an average of 81.6% (with M-ratio at 0.9) to about 80% at an M-ratio of 1.95. This can be largely attributed to the side reactions in the nitration process. The analysis of reaction products indicated that the side reactions mainly included carboxyl ortho-, para-position nitration and dinitration. As discussed above, the kinetically positive effects promoted both the main reaction and the side reactions simultaneously with the increase of M-ratio. Generally, carboxyl ortho- and para-position nitration reactions are considered to be parallel side reactions, and their reaction order is the same as the main reaction (Wen et al., 2017). Therefore, the effect of M-ratio on the selectivity became insignificant. At the same time, the dinitration of the etherate is believed to be a consecutive side reaction, which can be affected by M-ratio despite its high reaction activation energy (Chen et al., 2013). That led to the overall slight decrease in selectivity with raising M-ratio, as shown in Fig. 4(b).

3.2.3. Effects of varying total flow rate

With a given diameter of the reaction tube, varying total volumetric flow rate can affect the liquid–liquid two-phase hydrodynamics in the droplet-based reactor that may have potential impact on the reaction performance. This possible effect was examined by varying the total flow rate in a range of 200–1200 μL·min^{-1}. Accordingly, the main reaction tube length was changed in order to keep a constant residence time (83 s), while remaining N/S, M-ratio, organic phase concentration and reaction temperature all as constant. The reactant conversion and product selectivity as a function of total flow rate are depicted in Fig. 5.

It was observed that the conversion increased slightly from 65% to 67% with the increase of the total flow rate in the low total flow rate range (<426 μL·min^{-1}). That was followed by a slight decrease in conversion from 67% to 61% when the total flow rate was increased from 426 μL·min^{-1} to 580 μL·min^{-1}. As the total flow rate was raised further from 580 μL·min^{-1} to 1200 μL·min^{-1}, a very slight recovery of conversion was found, from 61% to 64%.

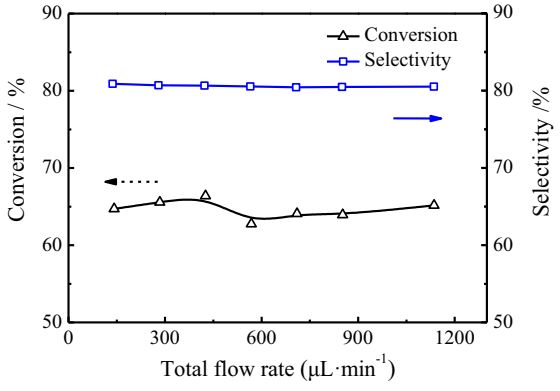

Fig. 5. Effects of the total flow rate and the reactor channel length. Etherate content in organic phase = 8.8 wt%, T = 298 K, residence time = 83 s, M-ratio = 1.6, N/S = 0.57.

The variation of reactant conversion was likely a result of the effect of total flow rate on the flow dynamic behavior of droplet-based microfluidics, such as geometry of dispersed droplets, their possible coalescence along the microchannel and two-phase interfacial property (Hao et al., 2020; Tang et al., 2013). Generally, at high total flow rates smaller dispersed droplets are formed that increased the interfacial surface area and, in turn, enhanced mass transfer performance leading to higher reaction rates. On the other hand, higher total flow rates can cause the coalescence of the dispersed acid droplets in microchannels, which can weaken the mass transfer performance. As observed in Fig. 6, the dispersion of the two-phase droplets was uniform and stable when the flow rate was below 426 μL·min^{-1}. In that case, the internal circulation in the droplets and the renewal velocity of two-phase phase interface were enhanced with the increase in the total flow rate, where the mass transfer rate from the organic phase to the acid droplets was intensified (Zhao et al., 2007; Antony et al., 2014), resulting in higher conversions. It can be seen in Fig. 6, with further increase in the flow rate, the coalescence of the dispersed droplets occurred causing the decrease of two-phase interfacial area and reduced mass transfer performance, despite the possible chaotic flow of the continuous phase at high flow rates (Husny and Cooper-White, 2006).

As shown in Fig. 5, the selectivity of the nitration reaction under these operating conditions remained approximately constant. This was largely due to the residence time, N/S, M-ratio, organic phase concentration and reaction temperature all being kept unchanged, which were considered to be the main factors affecting the selectivity of this reaction.

Overall, the effect of total flow rate was insignificant on either conversion or selectivity under the experiment conditions, suggesting a very wide operating zone which is beneficial for optimizing operation conditions and process scaling-up.

3.2.4. Effects of acetic anhydride content in organic phase

To investigate the effect of the addition of acetic anhydride, which has been found beneficial to the solubility of etherate in the organic phase and also acts as the water absorbent during the nitration reaction (Brown and Muxworthy, 1997; Brown et al., 1998; Brown et al., 2004). The addition of acetic anhydride has no other effects on the purification and separation of the product. During the reaction process, the etherate reacts with the mixed acid, and the product is dissolved in the solvent. The solid product is crystalized out by volatilizing the solvent and the acetic acid. Then, it is washed by soft water to remove the remained acid and other water-soluble impurities. Varying amount of acetic anhydride was introduced in a range of 0–8 wt% to the organic phase. The reactant conversion and product selectivity were measured under the reaction conditions of: 8.8 wt% etherate content in organic phase, 142 μL·min^{-1} total flow rate, N/S 0.57, M-ratio 1.6, and reaction temperature 298 K. The results are illustrated in Fig. 7.

It was initially interesting to observe that the conversion firstly decreased to a minimum level with the addition of acetic anhydride, dropping from approximate 98% to 77% when the acetic anhydride content was increased from 0 to 3 wt%. With further

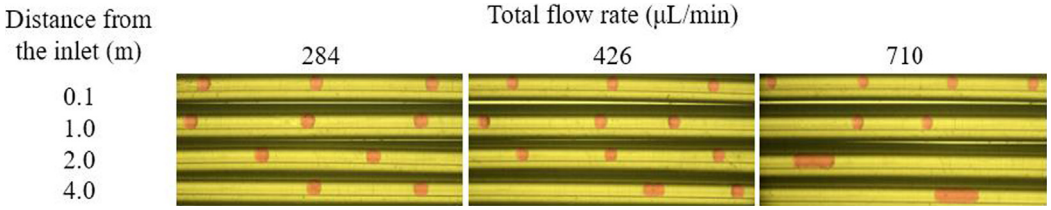

Fig. 6. Micrographs of the droplet flow under different operating conditions.

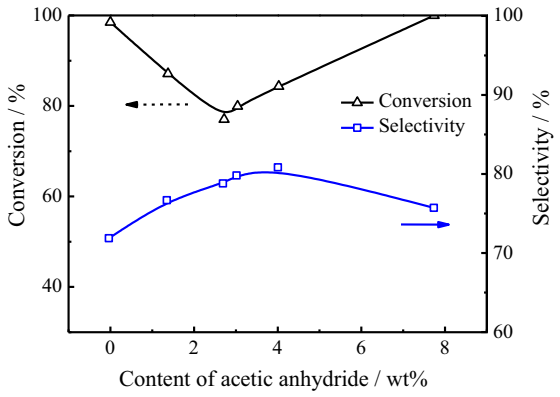

Fig. 7. Effects of acetic anhydride content in organic phase on nitration reaction.

increase in the acetic anhydride content from 3 wt% the conversion started to bounce back, until again approximate 100% when 8 wt% was added. At the same time, the curve of selectivity vs. acetic anhydride content exhibited an opposite trend to the conversion curve, showing a maximum selectivity of 80% at around 3 wt% acetic anhydride.

A closer examination revealed the critical role that acetic anhydride played with the solubility of etherate in the organic phase, mainly 1,2-dichloroethane. Without acetic anhydride added, the solubility of etherate was very low in 1,2-dichloroethane at 293–298 K, where even precipitation took place in the syringe. In this case, the amount of etherate fed into the reactor was in fact far from that expected, i.e. having a much higher M-ratio than the set value. Therefore, an apparent highest conversion close to 100% and a lowest selectivity of 72% were observed, that was in line with the results of the effect of M-ratio on the reaction, as shown in Fig. 4. By adding acetic anhydride the solubility of etherate was improved, until fully dissolved in 1,2-dichloroethane with 2.73 wt% of acetic anhydride added, where the minimum and maximum of conversion and selectivity were reached, respectively.

By further increasing the content of acetic anhydride, other roles started to play more significantly by acetic anhydride. The increase in overall conversion resulting from adding more acetic anhydride prompted the side reactions simultaneously, leading to the increase of dinitration by-products as detected from HPLC analysis. On the one hand, acetic anhydride can improve the dehydration of sulfuric acid in the mixed acid and the formation of NO_2^+ (Brown and Muxworthy, 1997). On the other hand, acetic anhydride can react with water from the nitration reaction to form acetic acid, which is also positive for generating NO_2^+. Finally, the existing NO_2^+ in the mixed acid increases the possibility of dinitration. This was also in line with the observation discussed above in Fig. 4.

3.3. Scalability study by varying microreactor geometry

To increase the reactor output, one of the commonly used approaches is to scale up the reactor capacity that is the reactor channel diameter in continuous flow microreactors. However, during the scaling-up of microreactors their unique characteristics need to be kept, such as microfluidic controllability, and mass and heat transfer properties. To understand the scalability of the droplet-base microreactor for the nitration reaction in this work, microreactors with three microchannel diameters (i.e. 0.5, 1.0 and 1.59 mm i.d.) were constructed to investigate the effect of varying reactor channel diameter on reactant conversion with a fixed N/S at 0.57, M-ratio at 1.6, and temperature at 298 K (Fig. 8).

As can be seen from Fig. 8(a), where both residence time (t = 333.5 s) and total flow rate (Q = 142 μL·min^{-1}) were kept constant by changing the reactor length (0.4–4 m) accordingly, the conversion of etherate decreased slightly from 80% to 75.5% with the increase of the inner diameter of the reactor tube from 0.5 mm to 1.59 mm. That was mainly due to the change of flow dynamics. As the residence time and the total flow rate were kept unchanged, the smaller inner diameter resulted in higher flow velocity, leading to more intense chaotic convection and more rapid interface renewal that were beneficial to the apparent reaction rate. In addition, the increase of inner diameter was more favorable for the occurrence of coalescence of the dispersed droplets, which further reduced the liquid–liquid two-phase interfacial area and increased the mass transfer distance.

Fig. 8(b) shows that, when both constant residence time (t = 333.5 s) and capillary length were kept constant (4 m) by varying the total flow rate (Q = 142–1448 μL·min^{-1}), the conversion decreased from 80% to 58.4% with the increase of the reactor tube diameter from 0.5 mm to 1.59 mm. This was likely related to the increased mass transfer distance between the two phases in larger diameter reactors, again due to the higher probability of coalescence of the adjacent dispersed droplets. Moreover, the higher total flow rate required for the larger diameter reactor led to more intense droplet coalescence, thus the reduced phase interfacial area further affected negatively the transport efficiency and decrease the overall conversion. Nevertheless, the results were indicative that, under the given experimental conditions, with a slight decrease in reactant conversion (e.g. from 80% to 70%) it

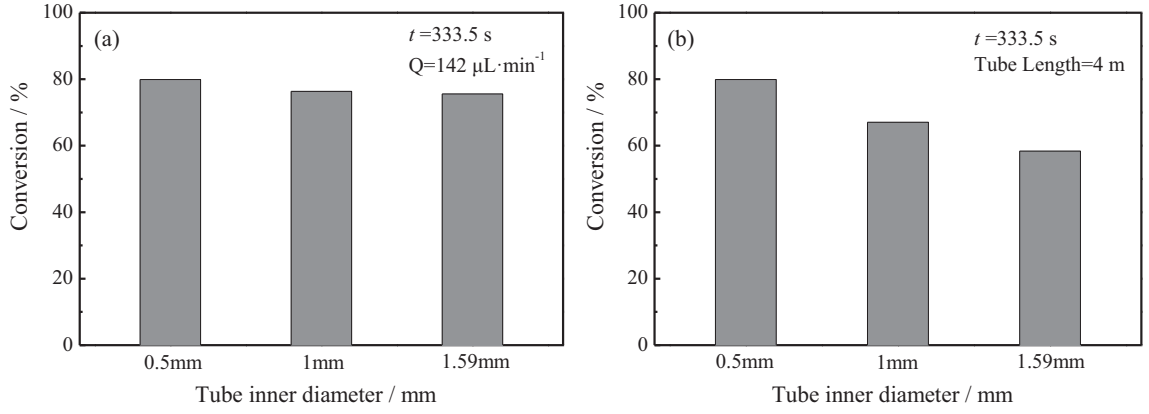

Fig. 8. Effect of the tube inner diameter on etherate conversion. Etherate content in organic phase = 8.8 wt%, N/S = 0.57, M-ratio = 1.6, T = 298 K.

was able to give a fourfold increase in total volumetric flow rate when the reactor channel diameter was doubled (from 0.5 mm to 1.0 mm).

3.4. Chemical kinetics

3.4.1. Apparent reaction rate

In the heterogeneous nitration process, the aromatic compounds diffuse to the liquid–liquid two-phase interface through the organic phase into the aqueous phase while nitration usually occurs in the interface boundary layer and/or in the aqueous phase (Zaldivar et al., 1995). Although the opposite diffusion of nitric acid and sulfuric acid to organic phase might occur, their solubility in the organic phase was very limited to form nitronium ions for nitration (Schöfield, 1980; Olah et al., 1989). While mass transfer and nitration reaction are difficult to be decoupled, a pseudo-homogeneous phase model has been proposed to cover the coupled two processes (Papayannakos and Petrolekas, 1992; Andreozzi et al., 1993). Based on experiment results in homogeneous nitration reactions, a second-order kinetics was adopted to correlate the reaction rate (r) with the concentration of reactants (Zaldivar et al., 1992; Andreozzi et al., 2006; Di Somma et al., 2012; Mandal et al., 2014), as expressed in Eq. (7).

$$r = k_{app} C_A C^t_{HNO_3} \tag{7}$$

where k_{app} is the apparent reaction rate constant, and C_A and $C^t_{HNO_3}$ are the concentration of etherate and nitric acid based on the total volume of mixed fluids, respectively. Eq. (7) can be further arranged as Eq. (8).

$$r = C^0_A \frac{dx_A}{dt} = k_{app}(C^0_A)^2(1-x_A)(M-x_A), M \neq 1 \tag{8}$$

where C^0_A is the initial concentration of etherate, x_A is the conversion of etherate, and M is the initial M-ratio. Integrating Eq. (8) yields Eq. (9) for determining product concentration parameter (G) at a given of time (t).

$$G = \frac{1}{C^0_A(M-1)} \ln\left[\frac{M-x_A}{M(1-x_A)}\right] = k_{app} t \tag{9}$$

Eq. (9) suggests that a plot of G vs. t should be linear passing through the origin with a slope equal to k_{app} under constant reaction temperature conditions. The initial concentration of etherate can be calculated with Eq. (10).

$$C^0_A = \frac{n_A}{v_{Organic} + v_{Mixed\ acid}} = \frac{v_{Organic}\rho_{Organic} w}{M_A(v_{Organic} + v_{Mixed\ acid})} \tag{10}$$

where n_A is the amount of substance of etherate; $v_{Organic}$ and $v_{Mixed\ acid}$ are the flow rates of organic phase and mixed acid, respectively. M_A denotes the relative molecular mass of etherate, and $\rho_{Organic}$, the density of etherate. w is the mass fraction of etherate in organic phase.

To determine the apparent reaction rate constant k_{app}, in this work the kinetic experiments were conducted at four temperature levels (i.e. 288, 298, 308 and 318 K) with four compositions of mixed acid where the sulfuric acid concentration were 11.30, 12.09, 12.42 and 13.53 mol·L^{-1}. The experiments were carried out at high flow rate, and the total flow rate of organic phase and mixed acid phase was set as 845–3380.7 μL·min^{-1}. The measured parameters (G) as a function of reaction time (t) are plotted in Fig. 9. It can be seen that the excellent linear relations were obtained under the given operating conditions, supporting the assumption of a second-order reaction.

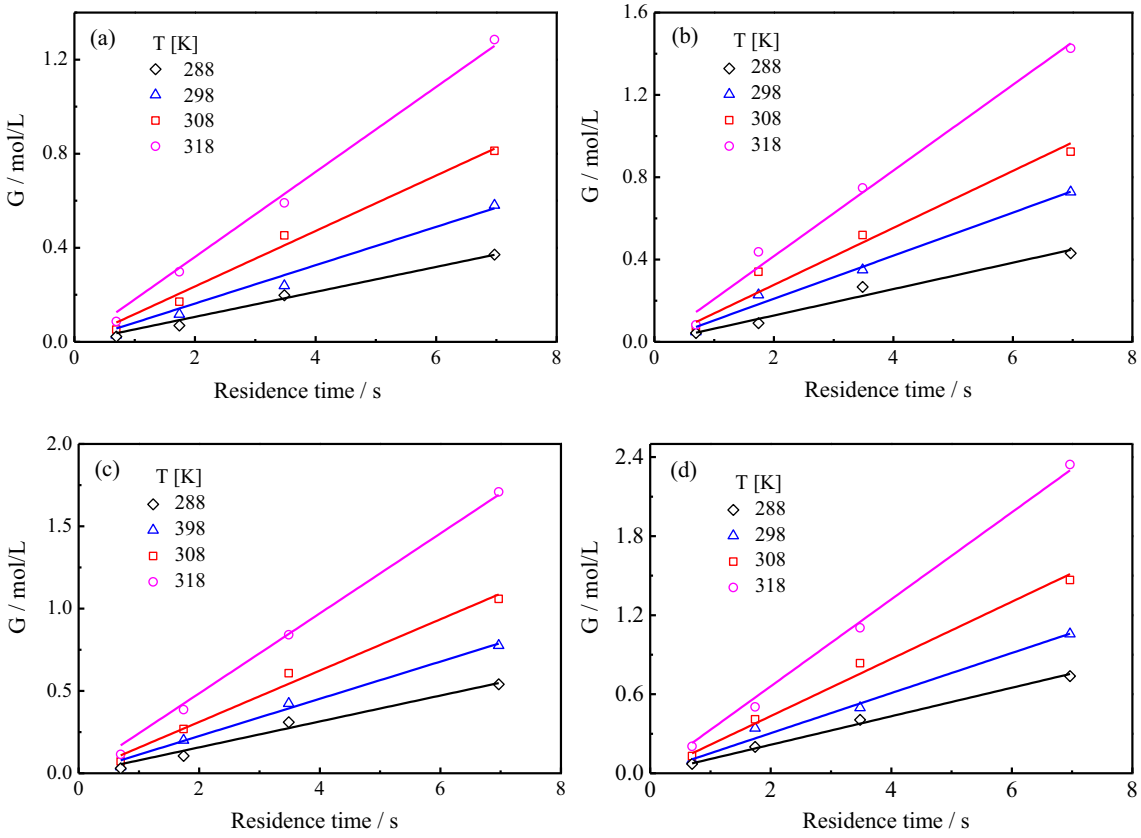

Fig. 9. Determination of apparent rate constants by keeping constant M-ratio = 1.6. (a) Concentration of sulfuric acid = 11.3 mol·L^{-1}, N/S = 0.75; (b) concentration of sulfuric acid = 12.09 mol·L^{-1}, N/S = 0.62; (c) concentration of sulfuric acid = 12.42 mol·L^{-1}, N/S = 0.57; (d) concentration of sulfuric acid = 13.53 mol·L^{-1}, N/S = 0.41.

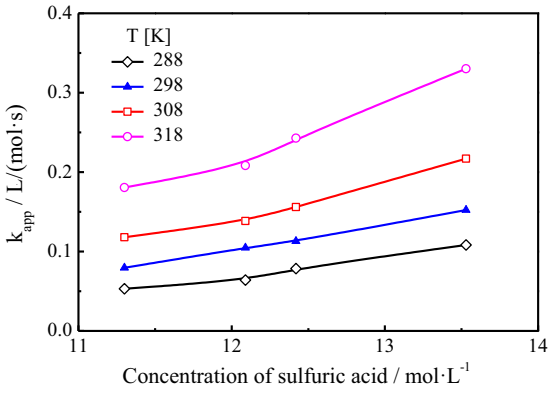

Fig. 10. Variation of experimental values of k_{app} with different sulfuric acid concentrations in mixed acid at different temperature levels.

Fig. 10 shows the relationship between k_{app} and sulfuric concentration of the mixed acid at different temperatures. It can be seen that, k_{app} increased with the increase of the concentration of the sulfuric acid at each temperature level, and also with the increase of the reaction temperature. This was in agreement with the previous observation for the effects of temperature, M-ratio and N/S on overall reaction performance (Fig. 3&4).

3.4.2. Intrinsic reaction rate

The rate-determining step of the nitration reaction between the mixed acid and the aromatic compounds in aqueous phase is believed to be the attack of the nitronium ion NO_2^+ on the aromatic compounds (Albright and Hanson, 1976; Marziano et al., 1984; D'Angelo et al., 2003), where NO_2^+ is the real nitrating agent instead of HNO_3. Therefore, the reaction rate can be further expressed in terms of concentrations of etherate and nitronium ion (Eq. (11)).

$$r = k^*_{exp} C_A C_{NO_2^+} \tag{11}$$

where k^*_{exp} and $C_{NO_2^+}$ are the apparent rate constant and the concentration of the nitronium ion in the mixed acid phase, respectively. According to the transition-state theory (Olah et al., 1989), the reaction rate equation can be expressed as Eq. (12).

$$r = k_0 C_A C_{NO_2^+} \frac{\gamma_A \gamma_{NO_2^+}}{\gamma^*} \tag{12}$$

where k_0 is the intrinsic reaction rate constant, which only depends on temperature. γ_A and $\gamma_{NO_2^+}$ are the activity coefficients of etherate and NO_2^+, respectively. γ^* is the activity coefficient of the transition-state intermediate.

Since there has been no accurate experimental data for obtaining these activity coefficients, M_c function (activity coefficient function) proposed by Marziano et al. (Marziano and Sampoli, 1983; Marziano et al., 1973; Marziano et al., 1981) was used in this work to describe the relationship between the activity and the sulfuric acid acidity. The rate equation is rewritten as Eq. (13).

$$r = k_0 C_A C_{NO_2^+} \, 10^{-nM_c} \tag{13}$$

where n is the thermodynamic parameter associated with aromatic compounds, and the value of n is unique for each aromatic compound. The sulfuric acid acidity was expressed by M_c function, and the value of M_c was determined only by the concentration of the acid at a given temperature. The quantity 10^{-nM_c} describes the relation of the ratio of the activity coefficients and the sulfuric acid concentration.

By combining Eqs. (7) & (11), the relation between k^*_{exp} and k_{app} can be obtained.

$$k^*_{exp} = \frac{k_{app} C^t_{HNO_3}}{C_{NO_2^+}} \tag{14}$$

Further, the relation of k_0 with k_{app} can be obtained from Eqs. (11), (13) and (14).

$$k_0 = \frac{k_{app} C^t_{HNO_3}}{C_{NO_2^+} \, 10^{-nM_c}} \tag{15}$$

Then, Eq. (15) is rearranged as Eq. (16).

$$\log k_{app} - \log(C_{NO_2^+} / C^t_{HNO_3}) = \log k_0 - nM_c \tag{16}$$

According to Eq. (16), a plot of $\log k_{app} - \log(C_{NO_2^+} / C^t_{HNO_3})$ vs. $-M_c$ should show a straight line, where n and $\log k_0$ can be determined from the slope and the intercept of the straight line, respectively. However, to calculate the values of n and k_0, M_c and the ratio of $C_{NO_2^+}$ to $C^t_{HNO_3}$ need to be necessarily determined firstly.

According to the values of M_c (298 K) at different sulfuric acid concentrations given by Marziano et al. (1981), an empirical correlation between the sulfuric acid concentration in the range of 11–14 mol·L^{-1} can be obtained by a polynomial fitting.

$$-M_c(298\ \text{K}) = -5.552 \times 10^{-4} C^4_{H_2SO_4} + 1.85 \times 10^{-2} C^3_{H_2SO_4} - 0.179 \times C^2_{H_2SO_4} + 1.11 \times C_{H_2SO_4} \tag{17}$$

For a given mixed acid composition, the values of M_c at different temperatures can be determined by the relationship proposed by Marziano (1998).

$$M_c(T) = M_c(298\ \text{K}) \left[\frac{200}{T} + 0.3292\right] \tag{18}$$

$(C_{NO_2^+} / C^t_{HNO_3})$ can be determined from the ionization equilibria of nitric acid in sulfuric acid (Rahaman et al., 2010). There are two different ionization equilibria for nitric acid coexisting simultaneously in aqueous sulfuric acid, which are the autoionization of nitric acid and the protonation of nitric acid by sulfuric acid, respectively, as shown in Eqs. (19) & (20).

$$HNO_3 \rightleftharpoons NO_3^- + H^+ \tag{19}$$

$$HNO_3 + H^+ \rightleftharpoons NO_2^+ + H_2O \tag{20}$$

The concentration of nitric acid in the reaction can be expressed as follows.

$$C^t_{HNO_3} = C_{NO_2^+} + C_{HNO_3} + C_{NO_3^-} \tag{21}$$

The equilibrium constants corresponding to Eqs. (19) & (20) can be written as.

$$K_{HNO_3} = \frac{a_{NO_3^-} \, a_{H^+}}{a_{HNO_3}} = \frac{C_{NO_3^-} \, C_{H^+}}{C_{HNO_3}} 10^{-n_{HNO_3} M_c} \tag{22}$$

$$K_{NO_2^+} = \frac{a_{HNO_3} a_{H^+}}{a_{NO_2^+} a_{H_2O}} = \frac{C_{HNO_3} C_{H^+}}{C_{NO_2^+} C_{H_2O}} 10^{-n_{NO_2^+} M_c} \tag{23}$$

The values of n_{HNO_3} and $n_{NO_2^+}$ obtained by Sampoli et al. (Sampoli et al., 1985) in the mixed acid are 0.571 and 2.542, respectively. The relationship between the two dissociation equilibrium constants and the reaction temperature can be expressed as Eqs. (24) & (25),

$$K_{HNO_3} = \exp\left(-\frac{\Delta G_{HNO_3}}{RT}\right) \tag{24}$$

$$K_{NO_2^+} = \exp\left(\frac{1.36 \times 10^4}{T} - 5.935\right) \tag{25}$$

where ΔG_{HNO_3} is 80.79 kJ·mol^{-1}, which denotes the Gibbs free energy of HNO_3 at 298 K. Zaldivar et al. (Zaldivar et al., 1995) obtained Eq. (24) by correlating the experimental data of Ross et al (Ross et al., 1983).

In the mixed acid, it can be generally assumed that the concentration of H^+ only depends on the sulfuric acid concentration, as the temperature fluctuation range is insignificant. The following empirical function was proposed by Zaldivar et al. (1995), based on the experimental data from Robertson and Dunford (1964), the proton concentration in aqueous sulfuric acid solution in the range of 1–99 wt% was correlated.

$$C_{H^+} = -1.1757\times10^{-2} + 1.2406C_{H_2SO_4} + 9.4286\times10^{-2}C^2_{H_2SO_4} - 2.5102\times10^{-2}C^3_{H_2SO_4} + 2.171\times10^{-3}C^4_{H_2SO_4} - 6.917\times10^{-5}C^5_{H_2SO_4} \quad (26)$$

According to Eqs. (16), (21), (22) and (23), the following form can be obtained.

$$\log Z = \log k_0 - nM_c \quad (27)$$

$$Z = k_{app}\left[\frac{K_{HNO_3}}{C_{H^+}10^{-n_{HNO_3}M_c}} + \frac{C_{H^+}10^{-n_{NO_2^+}M_c}}{C_{H_2O}K_{NO_2^+}} + 1\right]\times\frac{C_{H_2O}K_{NO_2^+}}{C_{H^+}10^{-n_{NO_2^+}M_c}} \quad (28)$$

According to Eq. (28), a straight line can be obtained by plotting logZ vs. -M_c, and the value of logk_0 can be calculated from the intercept, whilst n is the slope of the fitting line. As shown in Fig. 11, the linear relationship well fits the experimental data, where the parallel lines appear for different temperature, and n is independent of the reaction temperature and determined, being 0.1314.

With the value of k_0 obtained at different temperatures, the activation energy for the electrophilic attack of nitronium ion on the etherate can be determined by the Arrhenius equation (Eq. (29)).

$$k^0 = A\exp(-Ea/RT) \quad (29)$$

By plotting lnk_0 vs. 1/T in Fig. 12, the activation energy Ea and A (the pre-exponential factor) can be obtained from the slope and intercept of the straight line. By fitting the data of k_0 and t, the activation energy Ea was found to be 37.9 kJ·mol^{-1}, and A = 3.75 × 10^4 m^3/(mol·s).

3.4.3. Validation of pseudo-homogeneous phase assumption

In order to verify the pseudo-homogeneous phase assumption, the *Ha* number of the reaction process was calculated. The diffusivity of etherate ($D_{Etherate}$) in sulfuric acid was evaluated by the modified Wilke-Chang equation proposed by Perkins and Geankoplis (Schotte, 1992).

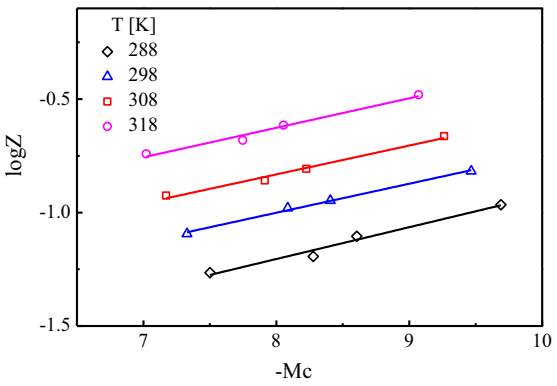

Fig. 11. Determination of the thermodynamic parameters n and k_0.

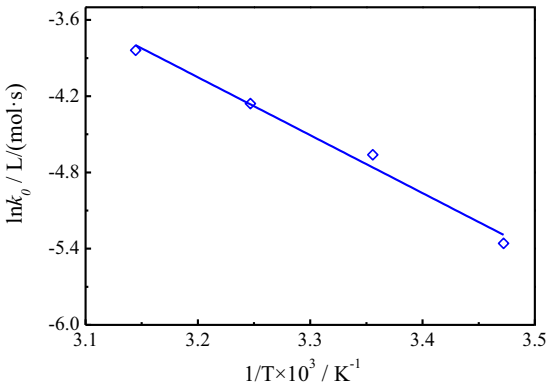

Fig. 12. Arrhenius plot of lnk_0 vs. 1/T.

$$D_{Etherate} = \frac{7.4\times10^{-8}T(\bar{\phi}\bar{M})^{1/2}}{\mu v_m^{0.6}} \quad (30)$$

where μ and v_m are the viscosity of sulfuric acid and the molecular volume of etherate at normal boiling point, respectively. $\bar{\phi}\bar{M}$ is defined as (Cox and Strachan, 1972):

$$\bar{\phi}\bar{M} = X_w\phi_wM_W + X_S\phi_SM_S \quad (31)$$

where the subscript w and s denote water and sulfuric acid, respectively. X,ϕ, and M are the mole fraction, the association factor, and the molecular weight, respectively. The diffusivity of etherate at different temperatures is presented in Table 1.

The value of k_L can be estimated using the dimensionless number of Sherwood, *Sh* (Rahbar-Kelishami and Bahmanyar, 2012) by Eq. (32), and Schmidt number and Reynolds number can be obtained by $Sc = \mu/\rho D_{Etherate}$ and $Re = \rho Du/\mu$. D and d are the diameters of microchannel and droplets, respectively. The *Ha* number is further calculated by Eq. (34).

$$Sh = \frac{k_Ld}{D_{Etherate}} = 0.991\times Pe^{1/3} \quad (32)$$

$$Pe = Re\times Sc \quad (33)$$

Table 1
Diffusivity of etherate in sulfuric acid and *Ha* number.

T (K)	$C_{H_2SO_4}$(mol·L^{-1})	$k_L\times10^{-3}$ (m·s^{-1})	$D_{Etherate}\times10^{-9}$ (m^2·s^{-1})	*Ha*
288	13.53	1.13	0.965	0.02686
	12.42	1.095	0.920	0.02590
	12.09	1.084	0.906	0.02416
	11.30	1.058	0.874	0.02358
298	13.53	1.455	1.41	0.02991
	12.42	1.409	1.34	0.02916
	12.09	1.395	1.32	0.02899
	11.30	1.361	1.28	0.02709
308	13.53	1.877	2.07	0.03351
	12.42	1.817	1.97	0.03214
	12.09	1.799	1.94	0.03128
	11.30	1.756	1.87	0.03095
318	13.53	2.304	2.81	0.03926
	12.42	2.231	2.68	0.03809
	12.09	2.209	2.64	0.03644
	11.30	2.155	2.54	0.03640

$$Ha = \frac{\sqrt{k_{app} D_{Etherate} C_{HNO_3}}}{k_L} \quad (34)$$

As shown in Table 1, $Ha < 0.3$ indicates that the etherate nitration with mixed acid took place in the slow regime and was kinetically controlled. The assumption of pseudo-homogeneous phase is reasonable.

3.4.4. Validation of kinetics models

Using the intrinsic reaction kinetics data for *Ea* and *A* obtained as described above, the values of apparent reaction rate constant k_{app} and reactant conversion can be computed according to Eq. (13). The calculated k_{app} and reactant conversions from the kinetics models are presented in Figs. 13 & 14 (continuous curves) under different reaction conditions with varying temperature, residence time, and sulfuric acid concentration. The experimentally measured results are also included in the figures for comparison. As can be seen from Figs. 13 & 14, the calculated data were reasonably in good agreement with the experimental results, validating the kinetics models developed.

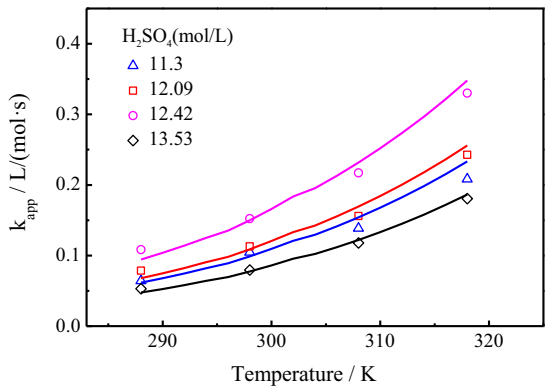

Fig. 13. Comparison of calculated (continuous lines) and experimental (symbols) results of k_{app} with varying temperature at different sulfuric acid concentration.

4. Conclusions

In the present work, the continuous flow nitration reaction of 3-[2-chloro-4-(trifluoromethyl) phenoxy] benzoic acid with a mixture of nitric and sulfuric acid was investigated within droplet-based microreactors. A wide range of operating parameters were examined to quantify their effects on the reaction outcome, including reaction temperature, residence time, M-ratio, N/S, total flow rate, composition of organic phase, and microreactor tube diameter. Furthermore, a pseudo-homogeneous based kinetics model was developed to determine the kinetics parameters of the nitration reaction, and the calculated data was validated against experimental results.

(1) Increasing reaction temperature and M-ratio results in overall higher reaction rate and conversion, and simultaneously increase in side reaction rate leading to the reduction of product selectivity, while increasing N/S reduces the conversion but has insignificant effect on product selectivity. The optimized reaction temperature, M-ratio and N/S are found to be 308 K, 1.6 and 0.57, respectively. Under optimal reaction conditions, a conversion of 83.03% and selectivity of 79.52% have been achieved in a microreactor (i.d. *d*= 0.5 mm, L = 4 m).

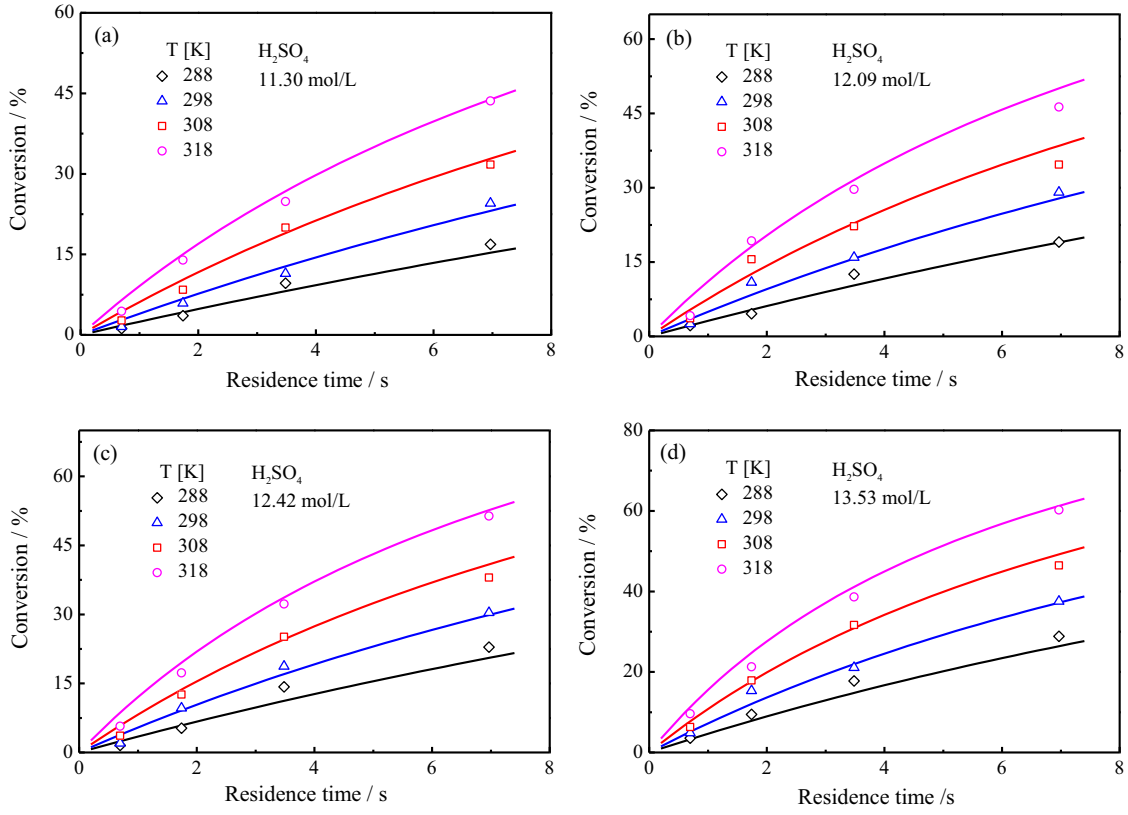

Fig. 14. Comparison of calculated (continuous lines) and experimental (symbols) results for the conversion of etherate with varying temperature.

(2) The effect of total flow rate was insignificant on either conversion (varying between 61% and 67%) or selectivity (varying between 80% and 81%) under the experiment conditions, suggesting a very wide operating zone which is beneficial for optimizing operation conditions and process scaling-up.
(3) The results from three reactor channel geometries (i.d. 0.5, 1.0 and 1.59 mm) were indicative that, under the given experimental conditions, with a slight decrease in reactant conversion (from 80% to 70%) it was able to give a fourfold increase in total volumetric flow rate when the reactor channel diameter was doubled (from 0.5 mm to 1.0 mm).
(4) The addition of acetic anhydride content can improve the solubility of etherate in the organic phase (mainly 1,2-dichloroethane) and the absorbability of water produced from the reaction, to inhibit the decrease of sulfuric acid strength while promote the generation of NO_2^+, leading to increase in conversion. With the increase of acetic anhydride content, however, the dinitration products increase accordingly, resulting in the reduction of the product selectivity.
(5) Pseudo-homogeneous based kinetics models have been developed of apparent reaction rate constant and intrinsic reaction rate constant for the reaction of 3-[2-chloro-4-(trifluoromethyl) phenoxy] benzoic acid with nitronium ion. Excellent linear relations are obtained and the apparent reaction rate is in compliance with the second-order reaction assumption, at given four temperature levels (i.e. 288, 298, 308 and 318 K) with four mixed acid compositions (concentration of sulfuric acid: 11.3, 12.09, 12.42 and 13.53 mol·L^{-1}). The values of *A* and *Ea* in the Arrhenius equation for this reaction are determined to be 3.75×10^4 m^3/(mol·s) and 37.9 kJ·mol^{-1}, respectively. The calculated results based on the kinetics model are in good agreement with the experimental results.

CRediT authorship contribution statement

Shenfang Li: Conceptualization, Investigation, Writing – original draft. **Xunli Zhang:** Methodology, Writing – review & editing. **Desheng Ji:** Methodology, Writing – review & editing. **Qingqiang Wang:** Supervision, Writing – review & editing. **Nan Jin:** Methodology. **Yuchao Zhao:** Supervision, Writing – review & editing.

Declaration of Competing Interest

The authors declare that they have no known competing financial interests or personal relationships that could have appeared to influence the work reported in this paper.

Acknowledgements

We gratefully acknowledge the financial supports from National Natural Science Foundation of China (Nos. 21978250, 21808194) and Natural Science Foundation of Shandong Province (ZR2020KB013, ZR2020QE211, 2019KJC012).

References

Albright, L.F., Hanson, C., 1976. Industrial and Laboratory Nitrations, Volume 22. ACS Symposium Series, Washington, DC.
Andreozzi, R., Canterino, M., Caprio, V., Di Somma, I., Sanchirico, R., 2006. Salicylic acid nitration by means of nitric acid/acetic acid system: chemical and kinetic characterization. Org. Process Res. Dev. 10 (6), 1199–1204.
Andreozzi, R., Insola, A., Aquila, T., Caprio, V., 1993. Kinetics of benzonitrile nitration with mixed acid under homogeneous conditions. Int. J. Chem. Kinet. 25 (9), 771–776.
Antony, R., Nandagopal, M.G., Sreekumar, N., Rangabhashiyam, S., Selvaraju, N., 2014. Liquid-liquid slug flow in a microchannel reactor and its mass transfer properties-a review. Bull. Chem. React. Eng. Catal. 9 (3), 207–223.
Brown, S.M., Gott, B.D., Muxworthy, J.P., 2004. Process for the preparation of diphenyl ether compound: U.S. Patent 6,790,991.
Brown, S.M., Muxworthy, J.P., 1997. Process for nitrating diphenyl ether compounds: WO. Patent 9,710,199. 1997-2-4.
Brown, S.M., Muxworthy, J.P., Lennon, M., Atherton, J.H., Preistley, I., 1998. Nitration process: WO. Patent 9,819,978. 1998-5-14.
Chen, Y.Z., Zhao, Y.C., Han, M., Ye, C.B., Dang, M.H., Chen, G.W., 2013. Safe, efficient and selective synthesis of dinitro herbicides via a multifunctional continuous-flow microreactor: one-step dinitration with nitric acid as agent. Green Chem. 15 (1), 91–94.
Coyle, E.E., Oelgemöller, M., 2008. Micro-photochemistry: photochemistry in microstructured reactors. The new photochemistry of the future? Photochem. Photobiol. Sci. 7 (11), 1313–1322.
Cox, P.R., Strachan, A.N., 1972. Two-phase nitration of toluene. Part II. Chem. Eng. J. 4 (3), 253–261.
Cui, Y.J., Song, J., Du, C.C., Deng, J., Luo, G.S., 2021. Determination of the kinetics of chlorobenzene nitration using a homogeneously continuous microflow. AIChE J. e17564.
D'Angelo, F.A., Brunet, L., Cognet, P., Cabassud, M., 2003. Modelling and constraint optimisation of an aromatic nitration in liquid-liquid medium. Chem. Eng. J. 91 (1), 75–84.
Deno, N.C., Peterson, H.J., Sacher, E., 1961. Nitric acid equilibria in water-sulfuric acid. J. Chem. Phys. 65 (2), 199–201.
Di Somma, I., Marotta, R., Andreozzi, R., Caprio, V., 2012. Kinetic and safety characterization of the nitration process of methyl benzoate in mixed acid. Org. Process Res. Dev. 16 (12), 2001–2007.
Giacobbe, T.J., Tsien, G., 1983. Process for recovering and purifying herbicidal phenoxybenzoic acid derivatives: US. Patent 4,405,805.
Hao, Y.Y., Jin, N., Wang, Q.Q., Zhou, Y.F., Zhao, Y.C., Zhang, X.L., Lv, H.Y., 2020. Dynamics and controllability of droplet fusion under gas-liquid-liquid three-phase flow in a microfluidic reactor. RSC Adv. 10 (24), 14322–14330.
Hessel, V., Cortese, B., De Croon, M., 2011. Novel process windows-concept, proposition and evaluation methodology, and intensified superheated processing. Chem. Eng. Sci. 66 (7), 1426–1448.
Husny, J., Cooper-White, J.J., 2006. The effect of elasticity on drop creation in T-shaped microchannels. J. Non-Newton Fluid Mech. 137 (1–3), 121–136.
Illg, T., Löb, P., Hessel, V., 2010. Flow chemistry using milli-and microstructured reactors-from conventional to novel process windows. Bioorganic Med. Chem. Lett. 18 (11), 3707–3719.
Jähnisch, K., Hessel, V., Löwe, H., Baerns, M., 2004. Chemistry in microstructured reactors. Angew. Chem. Int. Ed. 43 (4), 406–446.
Jiang, C.Y., 2006. Synthesis of concentrated technical grade fomesafen. Agrochemicals 2, 99–101.
Jin, N., Yue, J., Zhao, Y.C., Lv, H.Y., Wang, C.X., 2021. Experimental study and mass transfer modelling for extractive desulfurization of diesel with ionic liquid in microreactors. Chem. Eng. J. 413, 127419.
Kim, D.S., Lee, S.W., Kwon, T.H., Lee, S.S., 2004. A barrier embedded chaotic micromixer. J. Micromech. Microeng. 14 (6), 798–805.
Kulkarni, A.A., Kalyani, V.S., Joshi, R.A., Joshi, R.R., 2009. Continuous flow nitration of benzaldehyde. Org. Process Res. Dev. 13 (5), 999–1002.
Lan, Z., Lu, Y.C., 2021. Continuous nitration of o-dichlorobenzene in micropacked-bed reactor: process design and modelling. J. Flow Chem. 11 (2), 171–179.
Li, L., Yao, C.Q., Jiao, F.J., Han, M., Chen, G.W., 2017. Experimental and kinetic study of the nitration of 2-ethylhexanol in capillary microreactors. Chem. Eng. Process. 117, 179–185.
Ma, H.Y., Jin, N., Zhang, P., Zhou, Y.F., Zhao, Y.C., Zhang, X.L., Liu, J., 2019. Dynamic characterization of nanoparticles production in a droplet-based continuous flow microreactor. Chem. Eng. Res. Des. 144, 247–257.
Mandal, A.K., Kunjir, G.M., Singh, J., Adhav, S.S., Singh, S.K., Pandey, R.K., Kantam, M.L., 2014. Optimization of ammonium sulfamate nitration for the preparation of ammonium dinitramide. Cent. Eur. J. Energetic Mater. 11 (1), 83–97.
Marziano, N.C., Cimino, G.M., Passerini, R.C., 1973. The M_c activity coefficient function for acid-base equilibria. Part I. New methods for estimating pK_a values for weak bases. J. Chem. Soc. Perkin Trans. 2, 1915–1922.
Marziano, N.C., Tomasin, A., Traverso, P.G., 1981. The M_c activity coefficient function for acid-base equilibria. Part 5. The M_c activity coefficient for a reliable estimate of thermodynamic values. J. Chem. Soc. Perkin Trans. 2, 1070–1075.
Marziano, N.C., Sampoli, M., 1983. A simple linear description of rate profiles for the nitration of aromatic compounds in the critical range 80–98 wt% sulphuric acid. J. Chem. Soc. Chem. Commun. 523–524.
Marziano, N.C., Sampoli, M., Pinna, F., Passerini, A., 1984. Thermodynamic nitration rates of aromatic compounds. Part 2. Linear description of rate profiles for the nitration of aromatic compounds in the range 40–98 wt% sulphuric acid. J. Chem. Soc. Perkin Trans. 2, 1163–1166.
Marziano, N.C., 1998. Thermodynamic nitration rates of aromatic compounds. Part 4. Temperature dependence in sulfuric acid of $HNO_3 \rightarrow NO_2^+$ equilibrium, nitration rates and acidic properties of the solvent. J. Chem. Soc. Perkin Trans. 2, 1973–1982.
McMullen, J.P., Jensen, K.F., 2011. Rapid determination of reaction kinetics with an automated microfluidic system. Org. Process Res. Dev. 15 (2), 398–407.
Olah, G.A., Malhotra, R., Narang, S.C., 1989. Nitration: Methods and Mechanisms. VCH Publishers, New York.
Papayannakos, N.G., Petrolekas, P., 1992. Kinetic studies of homogeneous nitration of toluene. Ind. Eng. Chem. Res. 31 (6), 1457–1461.

Rahbar-Kelishami, A., Bahmanyar, H., 2012. New predictive correlation for mass transfer coefficient in structured packed extraction columns. Chem Eng Res Des. 90 (5), 615–621.
Rahaman, M., Mandal, B., Ghosh, P., 2010. Nitration of nitrobenzene at high-concentrations of sulfuric acid: Mass transfer and kinetic aspects. AIChE J. 56 (3), 737–748.
Robertson, E.B., Dunford, H.B., 1964. The state of the proton in aqueous sulfuric acid. J. Am. Chem. Soc. 86 (23), 5080–5089.
Ross, D.S., Kuhlmann, K.F., Malhotra, R., 1983. Studies in aromatic nitration. 2. Nitrogen-^{14}NMR study of the nitric acid/nitronium ion equilibrium in aqueous sulfuric acid. J. Am. Chem. Soc. 105 (13), 4299–4302.
Sampoli, M., De Santis, A., Marziano, N.C., Pinna, F., Zingales, A., 1985. Equilibria of nitric acid in sulfuric and perchloric acid at 25 ℃ by Raman and UV spectroscopy. J. Chem. Phys. 89 (13), 2864–2869.
Schöfield, K., 1980. Aromatic Nitration. Cambridge University Press, Cambridge, UK.
Schotte, W., 1992. Prediction of the molar volume at the normal boiling point. Chem. Eng. J. 48 (3), 167–172.
Sharma, Y., Joshi, R.A., Kulkarni, A.A., 2015. Continuous-flow nitration of o-xylene: effect of nitrating agent and feasibility of tubular reactors for scale-up. Org. Process Res. Dev. 19 (9), 1138–1147.
Shepherd, M., Medlock, A.E., Dailey, H.A., 2013. Encyclopedia of Biological Chemistry, second ed. in Lennarz W.J., Lane, M.D.(Eds.), Academic Press., Waltham, pp. 544-549.
Song, J., Cui, Y.J., Sheng, L., Wang, Y.J., Du, C.C., Deng, J., Luo, G.S., 2022a. Determination of nitration kinetics of p-Nitrotoluene with a homogeneously continuous microflow. Chem. Eng. Sci. 247, 117041.
Song, J., Cui, Y.J., Luo, G.S., Deng, J., Wang, Y.J., 2022b. Kinetic study of o-nitrotoluene nitration in a homogeneously continuous microflow. React. Chem. Eng. 7 (1), 111–122.
Su, Y.H., Hessel, V., Noël, T., 2015. A compact photomicroreactor design for kinetic studies of gas-liquid photocatalytic transformations. AIChE J. 61 (7), 2215–2227.
Sun, W.X., Zhang, X.L., Yao, C.Q., Wang, Q.Q., Jin, N., Lv, H.Y., Zhao, Y.C., 2021. Hydrodynamic characterization of continuous flow of Pickering droplets with solid nanoparticles in microchannel reactors. Chem. Eng. Sci. 245, 116838.
Tang, J., Zhang, X.B., Cai, W.F., Wang, F.M., 2013. Liquid-liquid extraction based on droplet flow in a vertical microchannel. Exp. Therm. Fluid Sci. 49, 185–192.
Vogt, E.C., Whiting, G.T., Dutta Chowdhury, A., Weckhuysen, B.M., 2015. In: Advances in Catalysis. Academic Press, Salt Lake City, pp. 143–314.
Wang, K., Lu, Y.C., Xia, Y., Shao, H.W., Luo, G.S., 2011. Kinetics research on fast exothermic reaction between cyclohexanecarboxylic acid and oleum in microreactor. Chem. Eng. J. 169 (1–3), 290–298.
Wen, Z.H., Jiao, F.J., Yang, M., Zhao, S.N., Zhou, F., Chen, G.W., 2017. Process development and scale-up of the continuous flow nitration of trifluoromethoxybenzene. Org. Process Res. Dev. 21 (11), 1843–1850.
Wen, Z.H., Yang, M., Zhao, S.N., Zhou, F., Chen, G.W., 2018. Kinetics study of heterogeneous continuous-flow nitration of trifluoromethoxybenzene. React. Chem. Eng. 3 (3), 379–387.
Yu, Z.Q., Lv, Y.C., Yu, C.M., Su, W.K., 2013. A high-output, continuous selective and heterogeneous nitration of p-difluorobenzene. Org. Process Res. Dev. 17 (3), 438–442.
Zaborenko, N., Murphy, E.R., Kralj, J.G., Jensen, K.F., 2010. Synthesis and kinetics of highly energetic intermediates by micromixers: direct multistep synthesis of sodium nitrotetrazolate. Ind. Eng. Chem. Res. 49 (9), 4132–4139.
Zaldivar, J.M., Barcons, C., Hernandez, H., Molga, E., Snee, T.J., 1992. Modelling and optimization of semibatch toluene mononitration with mixed acid from performance and safety viewpoints. Chem. Eng. Sci. 47 (9–11), 2517–2522.
Zaldivar, J.M., Molga, E., Alos, M.A., Hernandez, H., Westerterp, K.R., 1995. Aromatic nitrations by mixed acid. Slow liquid-liquid reaction regime. Chem. Eng. Process. 34 (6), 543–559.
Zeibi Shirejini, S., Mohammadi, A., 2017. Halogen-lithium exchange reaction using an integrated glass microfluidic device: an optimized synthetic approach. Org. Process Res. Dev. 21 (3), 292–303.
Zhang, P., Yao, C.Q., Ma, H.Y., Jin, N., Zhang, X.L., Lv, H.Y., Zhao, Y.C., 2018. Dynamic changes in gas-liquid mass transfer during Taylor flow in long serpentine square microchannels. Chem. Eng. Sci. 182, 17–27.
Zhao, Y.C., Chen, G.W., Yuan, Q., 2007. Liquid-liquid two-phase mass transfer in the T-junction microchannels. AIChE J. 53 (12), 3042–3053.
Zhou, Y.F., Yao, C.Q., Zhang, P., Zhang, X.L., Lv, H.Y., Zhao, Y.C., 2020. Dynamic coupling of mass transfer and chemical reaction for Taylor flow along a serpentine microchannel. Ind. Eng. Chem. Res. 59 (19), 9279–9292.